Effect of reaction time on $LiMn_2O_4$ nanostructures prepared by modified chemical bath deposition method

Lehlohonolo F. Koao[1]*, Setumo V. Motloung[2], Tshwafo E. Motaung[3]

[1]*Department of Physics, University of the Free State (Qwa Qwa campus), Private Bag X13, Phuthaditjhaba, 9866, South Africa*
[2]*Department of Physics, Nelson Mandela Metropolitan University (NMMU), P. O. Box 77000, Port Elizabeth 6031, South Africa*
[3]*Department of Chemistry, University of Zululand, Private Bag X1001, KwaDlangezwa 3886, South Africa*

*Corresponding author

DOI: 10.5185/amlett.2018.2137
www.vbripress.com/aml

Abstract

$LiMn_2O_4$ (LMO) powders were prepared by modified chemical bath deposition method. The effect of reaction time on the structure, morphology and optical properties of LMO nanostructures were investigated. The reaction time was varied from 1 - 120 min. The X-ray diffraction (XRD) patterns of the powders correspond to the various planes of a cubic spinel LMO phase. It was observed that the secondary phases decreases with an increase in reaction time. The diffraction peaks increase in intensity with an increase in reaction time up to 10 min. The estimated average grain sizes calculated using the XRD spectra were found to be in the order of 60 ± 1 nm. The scanning electron microscope (SEM) image suggested that the reaction time influences the morphology of the prepared powders. The irregular nanoparticle increased in size with an increase in reaction time. The UV-Vis spectra showed a red shift with an increase in reaction time up to 10 min.

Keywords: $LiMn_2O_4$; CBD; reaction time; morphology.

Introduction

$LiMn_2O_4$ (LMO) has attracted great attention in recent years as a promising cathode material for rechargeable lithium-ion batteries (LIB's) based on environmental safety consideration and various attractive characteristics associated with it **[1-3]**. Moreover, its excellent stability might allow safe, large-scale applications such as hybrid vehicles and load-leveling. Nowadays people are looking for environment friendly cathode materials for the electric vehicle and hybrid electric vehicle applications **[4]**. It is well known that the electrochemical performance of LIB's is strongly affected by particle sizes, morphology, specific surface area, crystallinity and composition **[2,5]**. Lv *et al*. **[2]** was able to find that an increase in specific area with the decrease of particle size from 300-900 nm to 50-120 nm facilitated the improvement of electrochemical capacity and cycling. The electrochemical performance decreased when particle size was too small as the calcination temperature decreases **[2]**. Hwang *et al*. **[1]** reported that a decrease in particle size resulted in an increase in the charging and discharging of the cathode materials. Choi *et al*. **[5]** was able to announce that nanometer sized cathode powders suffer from high fading rates because of their large electrode and electrolyte interface areas and poor crystallinity. Lv *et al*. **[2]** was able to report that LIB's materials with too big or too small particle sizes displayed not very well electrochemical performance. Therefore, it is very significant to improve the performance of LIB's materials by controlling appropriate particle sizes **[2]**. Lv *et al*. **[2]** showed that the LMO nanoparticles synthesized at 150 °C have the highest electrochemical capacity with the average particle sizes from 50-120 nm **[2].** To achieve high rates of charge and discharge, it is very good to obtain submicron sized particles with uniform morphology and homogeneity. The effect of reaction conditions such as reaction temperature on crystal parameters should be further studied since they might remarkably affect the electrochemical performance **[2]**. Many techniques based on the solid state and solution process have been used to prepare LMO powders **[4, 6-7]**. In this study, the chemical bath deposition (CBD) method was employed due to its simplicity, cheap, low temperature and it gives better homogeneity. The aim of this paper was to investigate the effect of reaction time on the structure, morphology and optical properties of the LMO nanopowders. Yunlong *et al*. **[8]** prepared $LiFePO_4$/C cathode materials by a combination of co-precipitation and microwave heating and the influence of microwave heating time on the structure and electrochemical

performance of the materials was explored. The results showed that the $LiFePO_4$/C heated for 9 min has a pure olive-type phase and excellent electrochemical performance. However, there are scares reports on the effect of reaction times on LMO nanoparticles via the CBD method. Thus, in this study, the effects of the CBD reaction time on the structure, morphology and optical properties is reported. Our results revealed that the LMO synthesized at reaction time of 10 min shows high crystallinity.

Experimental details

Materials synthesis

All the chemicals used for the preparation of the nano-powders were of analytical grade. These includes lithium acetate $Li(CH_3COO)_2 \cdot 2H_2O$, manganese acetate $Mn(CHCOO)_3 \cdot 6H_2O$, and citric acid (CA) $C_8H_8O_7 \cdot H_2O$. CA solutions were used as the complexing agent and oxidizing medium. The precursor were prepared by dissolving 0.25 M of lithium acetate and 0.5 M of manganese acetate in 100 mL of deionized water in separate beakers. The 0.75 M CA was dissolved in 500 mL of deionized water. A magnetic stirrer was used to stir each solution overnight at room temperature to ensure a homogenous solution of the reagents. The chemical bath solution was prepared as follows: 10 mL of a lithium acetate and manganese acetate solutions were mixed. The mixture was stirred for 30 s and 40 mL of CA solution was added slowly drop-wise while continuously stirring for 5 min. The solution was transparent in colour. The volume ratio for lithium acetate, manganese acetate and CA solution was 1:1:4. Water bath was maintained to be at a constant temperature of 80 ºC. Various reaction times of CBD were varied between 5 - 120 min. It was observed that the colour of the solutions were transparent and the solutions amount decreased with an increase in reaction times. The solution was then placed in the furnace for 16 h at 90 °C. Then, the temperature of furnace was increased to 200 °C and a foamy powder was obtained after 2 h. The obtained powder was annealed at 800 °C for 6 h in air using the furnace. The samples were ready to be characterized using various characterization techniques.

Characterizations

The crystal structures of the samples were determined with a Bruker AXS Discover diffractometer with CuKa (1.5418 Å) radiation. Morphology and the chemical composition of the samples were analyzed using a JEOL JSM-7800F field-emission scanning electron microscope (FE-SEM) equipped with an energy dispersive X-ray spectrometer (EDS). For sample preparation for SEM measurements, the holder or stub was covered with double sided carbon (C) tape. The double sided C tape improve the conductivity and also prevent powder sample from falling-off the sample holder. The Raman measurements were done using a T64000 series II triple spectrometer system from HORIBA Scientific, Jobin Yvon Technology. The 514.3 nm laser line of a coherent Innova® 70C series Ar+ laser (spot size ~ 2 µm) with a resolution of 2 cm-1 in the range 200 cm^{-1} – 800 cm^{-1} was used. The measurements were obtained in a backscattering configuration with an Olympus microscope attached to the instrument (using an LD 50x objective). The laser power was set at 1.5 mW. An integrated triple spectrometer was used in the double subtractive mode to reject Rayleigh scattering and dispersed the light onto a liquid nitrogen cooled Symphony CCD detector. The optical measurements were carried out in the 200 - 800 nm wavelength range using a Perkin Elmer UV/Vis Lambda 20 Spectrophotometer.

Results and discussions

Fig. 1 shows the XRD patterns of the LMO samples synthesized at various reaction times (5-120 min). The XRD patterns of all the samples are in agreement with the standard pattern of cubic spinel LMO (JCPDS: 35-0782 with a = 8.247Å) **[4]**. All the samples are identified as a single pure phase of cubic spinel structure in the space group Fd-3m, with high crystallinity degrees. In Fig. 1 at reaction time of 5 min it is clear that there are secondary peaks (indicated by the star (*)) due to Mn_3O_4 (JCPDS no: 80-0382) and those secondary peaks diminished with an in increase in reaction times of the bath.

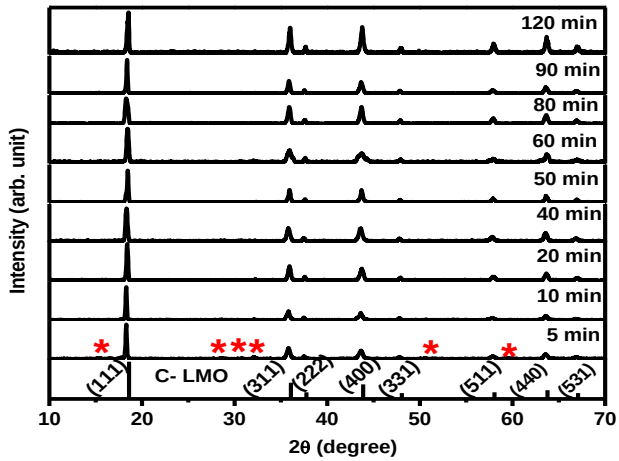

Fig. 1. XRD patterns of the prepared LMO powders at various reaction times.

Fig. 2 presents the analysis of the diffraction peak (111) of the prepared LMO nanopowders. It was observed that the diffraction peak intensity increased with an increase in the reaction time of CBD up to 10 min. This behavior suggests the improvement of crystalline quality during the growth of LMO powders. Above 10 min the diffraction peaks intensity decreases even though there are fluctuations. The decrease of the (111) diffraction peak intensity as the reaction time increases can be associated to the demolition of the crystalline quality, especially for sample synthesized at

120 min. Thus, varying the reaction time influences the crystallinity of the LMO powders. It can also be noted that above 10 min the diffraction peaks shifted to higher diffraction angles even though there are fluctuations. The shift and fluctuation of the diffraction angle indicates the possibilities of interchanging of Li (0.76 Å) and Mn (0.46 Å) on the crystal sites **[9-10]**. The average lattice parameters was calculated to be 8.297 Å, which matched perfectly with the standard data available in the JCPDS: 35-0782.

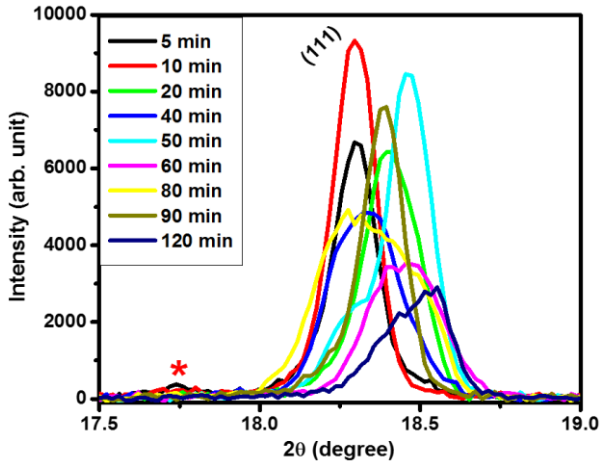

Fig. 2. The analysis of the main diffraction (111) peak.

The average crystallite size of the nanoparticles were estimated from all the XRD peaks line broadening using Scherrer's equation **[11]**. The results revealed that the crystallite size increased up to 10 min of reaction time of bath as shown in **Fig. 3**. The average crystallite size of the as prepared samples was estimated to be 60 ± 1 nm. Therefore, the observed increase in diffraction intensity up to 10 min (**see Fig. 2**) of reaction time is due to the increase in estimated crystallite size. For future investigations, note that the reaction time of 10 min will be considered for further experiment of LMO powder preparations.

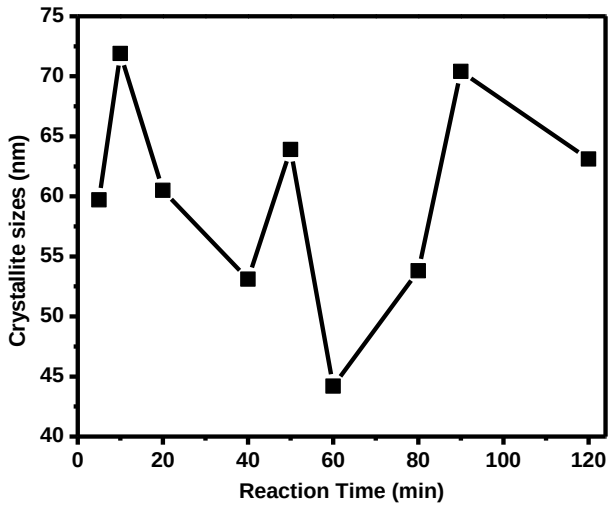

Fig. 3. The average crystallite sizes versus the reaction times of CBD method.

Fig. 4 (a)-(f) shows the SEM images of LMO nano-powders prepared at various reaction times. It can be observed that for all the images the particle are homogeneous distributed and aggregated. At the reaction time of 5 min as shown in **Fig. 4 (a)** the particle are found to be irregular in shape. In **Fig. 4(b)** for the sample synthesized at reaction time of 10 min it is clear that the particles are well defined and are polygon in shape. The crystallinity of the prepared LMO powders were reasonably good which agrees very well with the XRD analysis. Even in **Fig. 4 (c-d)**, the particles a polygon in shape, but for the samples synthesized at reaction times of 90 and 120 min as shown in **Fig. 4 (e-f)**, the polygon shape and crystallinity seems to have destroyed. This behaviour may be due to the decreasing of XRD peak intensity as observed from **Fig. 2**. Thus, the results suggest that the increase in reaction time changes the surface morphology of the prepared phosphor.

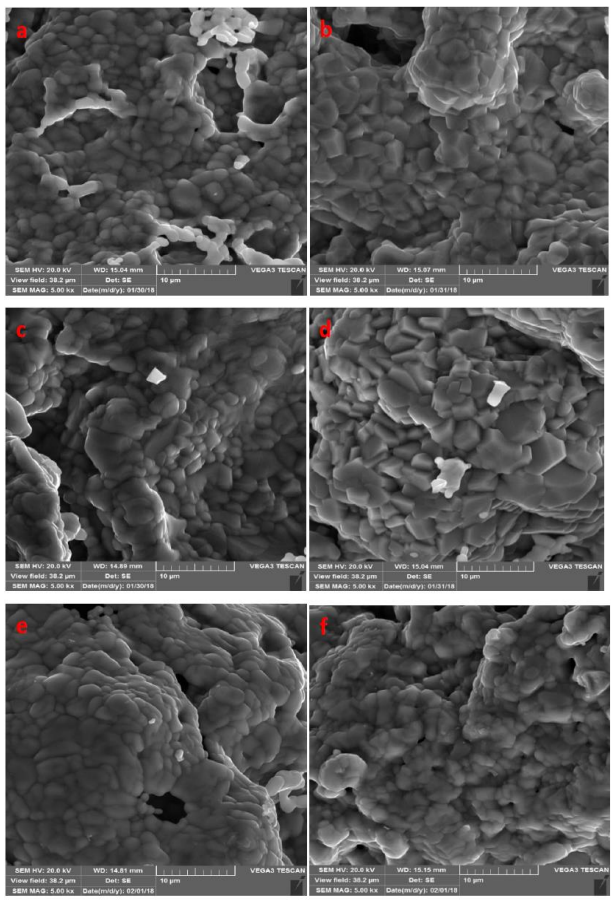

Fig. 4. The SEM images of LMO prepared at various reaction times (a) 5, (b) 10, (c) 40, (d) 50, (e) 90 and 120 min.

Elemental analysis of LMO nano-powders were conducted by EDS and elementary mapping analysis. The EDS result of the powders confirms the presence of Mn, O and C as shown in **Fig. 5 (a)-(c)**. Li is not detected by the EDS because of its low activation energy. The EDS spectra show an additional peak of carbon (C) present in all samples and that is attributed to the sample coating during EDS measurements.

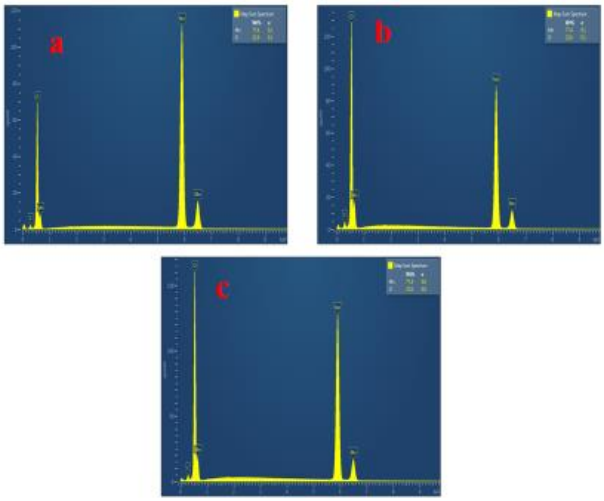

Fig. 5. (a) The EDS curves for LMO nanostructures prepared at various reaction time of (a) 10, (b) 50, and (c) 120 min.

Fig. 6 shows the elemental mapping of Mn and O, respectively. The EDS mapping for the samples synthesized at reaction time of 10 min results presented in **Fig. 6**, it is shows that the Mn and O were homogeneously dispensed on the surface. Note that similar maps (not shown here) were observed for the other samples.

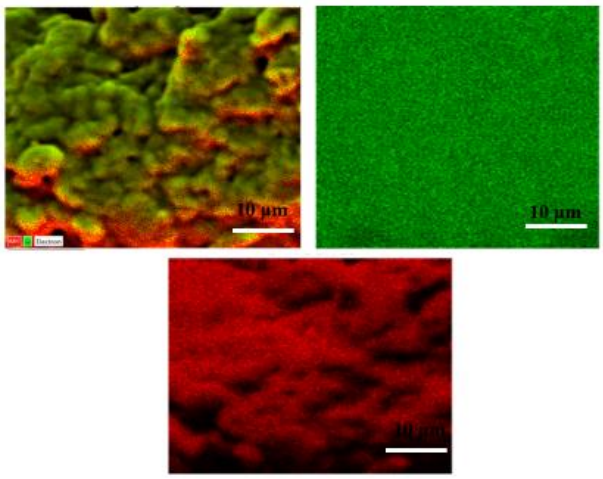

Fig. 6. The EDS legend image overlay for LMO nano-powders after elemental mapping for sample prepared at reaction times of 10 min which shows Mn (red) and O (green).

To investigate the vibrational modes and the phase purity of the LMO nanostructures, the Raman scattering method was employed. **Fig. 7** shows the normalized Raman scattering spectra of the LMO nanostructures prepared at different reaction times. For all spectra, a prominent peak at 613 cm^{-1} is observed. This peak is attributed to the A1g mode in the symmetry **[12]**. The band is characteristic of LMO spinel phase **[13]**. In addition, less intense peaks at between 200 and 520 cm^{-1} are common features of the LMO spectra. These bands can be assigned to the vibrational motion of oxygen atoms inside the octahedral MnO_6 unit **[14]**. The presence of Mn-O bands confirms that the sample has a spinel structure. The F_2g mode at around 356 cm^{-1} was ascribed to the Li-O vibration, which has a connection to the tetrahedral cation movements **[12]**. The low intensity band observed at 271 cm^{-1} might be related to the cationic disorder in the material **[12]**. By comparing all spectra it can be observed that the Raman peaks become more prominent for the sample synthesized at reaction temperature of 10 min. The observed behavior may be attributed to increased crystallite size effect for the sample synthesized at reaction time of 10 min. This further suggest the improvement in crystallinity of the material as observed in XRD results. The change in grain size have been observed to affects the vibrational properties **[15]**. Raman scattering is also sensitive to crystal symmetry and disorders in micro-and nano-crystalline structures due to defects/impurities **[16]**. Raman results agrees very well with the XRD results, which indicates the successful synthesis of LMO powders at various reaction times using CBD method.

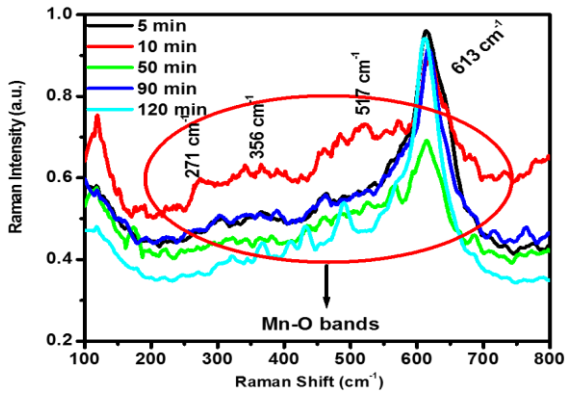

Fig. 7. (a) The Raman spectra of the LMO nano-powders prepared at various reaction times.

The UV-visible reflectance spectra of the LMO powders synthesized at various reaction times is illustrated in **Fig 8**. There is absorption band at around 350 nm with absorption onset at around 470 nm. The absorption band at around 350 nm circled with red colour may be due to the MnO nanoparticles. The absorption edge of the bulk MnO is around 320 nm **[17]**. It can be noted that the absorption edges slightly shifted to higher wavelengths for sample synthesized for 10 min as compared to other samples.

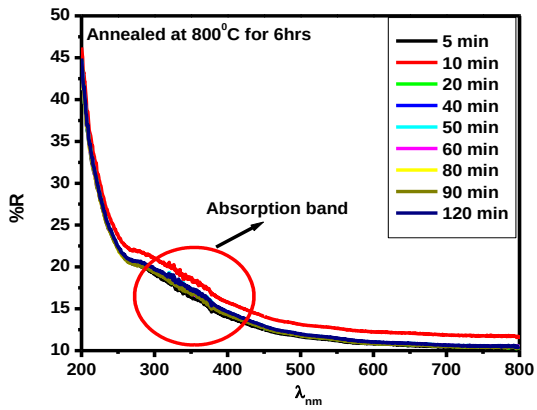

Fig. 8. The reflectance spectra of the LMO nanoparticles prepared at various reaction times.

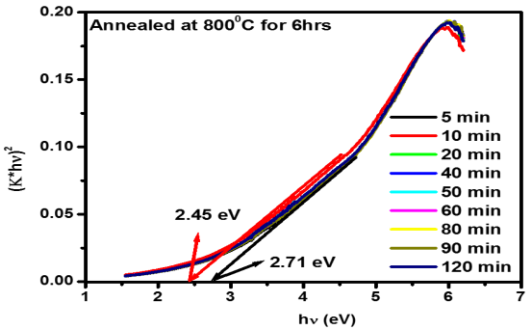

Fig. 9. Plot of (K*$h\nu$)^n versus ($h\nu$) which was used to determine the band gap energy of LMO powders synthesized at various reaction times.

Fig. 9 shows diffuse reflectance spectra for the various reaction time following Kubelka–Munk transformation **[9-10].** The band-gaps determined by linear extrapolation. The energy gap (E_g) value for the LMO sample synthesized at 10 min is 2.45 eV. The estimated average (E_g) for all the samples synthesized at various reaction times is 2.59 eV. The (E_g) are consistence with the literature values by other researchers **[17-18]**. It can be seen that the energy gap (E_g) of the LMO nanoparticles slightly decreased up to reaction time of 10 min. The slightly red shift of the absorption edges and reduction of E_g may be related to the estimated crystallite sizes that have been observed to increase when the reaction time of the CBD was increased up-to 10 min as confirmed on the XRD results **[19]**. In addition, the red shift may be due to lattice strain induced by the lattice distance that could lead to some shift in reflectance wavelength and the E_g. A possible explanation for this decrease in E_g with increase of the crystallite size is that the bulk defects excite the molecular orbitals in the conduction band edge and causes the red-shift of the absorption spectra **[20]**.

Conclusion and future perspectives

LMO powders were successfully synthesized at various reaction times by the modified CBD process. The formation of LMO nanoparticles was confirmed by XRD. XRD pattern revealed the LMO nanoparticles which belonged to the cubic spinel structure. It was found that the LMO sample synthesized for reaction time of 10 min showed high diffraction intensity. SEM showed that the surface morphology of the prepared nanopowders is influence by the CBD reaction time during synthesis. The EDS revealed the presence of the Mn and O, which are homogenously distributed over the surface. It was found that the Raman spectra confirmed the formation of LMO spinel by varying the reaction time of the CBD. Uv-vis analysis revealed that there was a slightly red shift up to 10 min reaction time. It was found that best reaction time of CBD for synthesizing LMO nanoparticles with high crystalline structure and well modified shape is 10 min. For future investigations, the 10 min reaction time will be kept constant while varying other experimental parameters in LMO synthesis.

Acknowledgements

This work is supported by the South African National Research Foundation (NRF) Thuthuka Programme (fund number: UID99224) andthe University of the Free State.

Author's contributions

Authors have no competing financial interests. They have modified the paper.

References

1. Hwang, B. J.; Santhanam, R.; Liu, D. G. *J. Power. Source.*, **2001**, *97-98*, 443-446. **DOI:** 10.1016/S0378-7753(01)00635-8
2. Lv, X.; Chen, S.; Chen, C.; Liu, L.; Liu, F.; Qiu, G., *Solid. State. Sci*. **2014**, *31*, 16-23. **DOI:** 10.1016/j.solidstatesciences.2014.02.015.
3. Tanaka, M.; Kageyama, T.; Sone, H.; Yoshida, S.; Okamoto D.; and Watanabe, T., *Nanomaterials*, **2016**, *60(6)*, 9. **DOI:** 10.3390/nano6040060.
4. Zhou, X.; Chen, M.; Bai, H.; Su, C.; Feng, L.; Guo, J. *Vacuum*, **2014**, *99*, 49-55. **DOI:** 10.1016/j.vacuum.2013.04.011
5. Choi, S.H.; Kim, J. H.; Ko, Y.N.; Kang, Y.C.; *Int. J. Electrochem. Sci*., **2013**, *8*, 1146-1162.
6. Guler, M.O.; Akbulut, A.; Cetinkaya, T.; Uysal, M.; Akbulut, H. *International Journal of Hydrogen Energy*, **2014**, *39*, 21447-21460 **DOI:** 10.1016/j.ijhydene.2014.04.107
7. Ragavendran, K. R.; Xia, H.; Yang, G.; Vasudevan, D.; Emmanuel, B.; Sherwood, D.; Arof, A. K., *Phys. Chem. Chem. Phys*., **2014**, *16*, 2553. **DOI:** 10.1039/c3cp54439g
8. Yunlong, X. U.; Lili, T.; Hongyan, M.A.; Huaqing, H, *Front. Chem. Eng. China*, **2008**, *2(4)*, 422–427. **DOI:** 10.1007/s11705-008-0082-4
9. Motloung, S.V.; Dejene, F.B.; Kroon, R.E.; Ntwaeaborwa, O.M.; Swart, H.C.; Motaung, T.E., *Opt. Mater*., **2017**, *131*, 705-712. **DOI:** 10.1016/j.ijleo.2016.11.165
10. Motloung, S.V.; Dejene, F.B.; Sithole, M.E.; Koao, L.F.; Ntwaeborwa, O.M.; Swart, H.C.; Motaung. T.E., *J. Electr. Mater*., **2016**, *45*, 4796. **DOI:** 10.1007/s11664-016-4660-9.
11. Lavand A. B.; Malghe Y. S. *Adv. Mater. Lett*. **2015**, *6(8)*, 700. **DOI:** 10.5185/amlett.2015.5800
12. Rao, B. N.; Muralidharan, P.; Kumar, P. R.; Venkateswarlu, M.; Satyanarayana, N., *Int. J. Electrochem. Sci.*, **2014**, *9*, 1207 – 1220.
13. Lin, B.; Yin, Q.; Hu, H.; Lu, F.; Xia, H.; *J. Solid State Chem*., **2014**, *209*, 23-28. **DOI:** 10.1016/j.jssc.2013.10.016
14. Rangappa, D.; Mohan, E. H.; Siddhartha, V.; Gopalan, R.; and Rao, T. N, *AIMS Materials Science*, **2014**, *1(4)*, 174-183. **DOI:** 10.3934/matersci.2014.4.174
15. Yadav, K.; Jaggi, N., *J Mater Sci: Mater Electron*, **2016**, *27*, 393–398. **DOI:** 10.1007/s10854-015-3766-9
16. Kumaria, R.; Sahai, A.; Goswami, N., *Progress in Natural Science:Materials International*, **2015**, *25*, 300–309. **DOI:** org/10.1016/j.pnsc.2015.08.003
17. Vijayamari, A.; Sadayandi, K.; Sagadevan, S.; Singh, P.; *J. Mater Sci: Mater Electron*, **2017**, *28*, 2739–2746. **DOI:** 10.1007/s10854-016-5853-y
18. Nouri, J.; Khoshravesh, T.; Khanahmadzadeh, S.; Salehabadi, A.; Enhessari, M., *Int. J. Nano Dimens.*, **2016**, *7(1)*, 15-24. **DOI:** 10.7508/IJND.2016.01.002
19. Sahu, S. N.; Nanda, K. K., *Proc. Indian Natl. Sci. Acad*., **2001**, *67 (A)*, 103–130.
20. Abbasi, A.; Mirhabibi, A.; Arabi, H.; Golmohammad, M.; Brydson, R., *J. Mater. Sci: Mater Electron*, **2016**, *27*, 7953–7961. **DOI:** 10.1007/s10854-016-4788-7

